Impact of P-Glycoprotein Function on the Brain Kinetics of the Weak Substrate ^{11}C-Metoclopramide Assessed with PET Imaging in Humans

Nicolas Tournier*[1], Martin Bauer*[2], Verena Pichler[3], Lukas Nics[3], Eva-Maria Klebermass[3], Karsten Bamminger[2,3], Peter Matzneller[2], Maria Weber[2], Rudolf Karch[4], Fabien Caillé[1], Sylvain Auvity[1], Solène Marie[1], Walter Jäger[5], Wolfgang Wadsak[3,6], Marcus Hacker[3], Markus Zeitlinger[2], and Oliver Langer[2,3,7]

[1]UMR 1023 IMIV, Service Hospitalier Frédéric Joliot, CEA, Inserm, Université Paris Sud, CNRS, Université Paris-Saclay, Orsay, France; [2]Department of Clinical Pharmacology, Medical University of Vienna, Vienna, Austria; [3]Division of Nuclear Medicine, Department of Biomedical Imaging and Image-Guided Therapy, Medical University of Vienna, Vienna, Austria; [4]Centre for Medical Statistics, Informatics, and Intelligent Systems, Medical University of Vienna, Vienna, Austria; [5]Department of Clinical Pharmacy and Diagnostics, University of Vienna, Vienna, Austria; [6]Center for Biomarker Research in Medicine—CBmed GmbH, Graz, Austria; and [7]Biomedical Systems, Center for Health & Bioresources, AIT Austrian Institute of Technology GmbH, Seibersdorf, Austria

PET with avid substrates of P-glycoprotein (ABCB1) provided evidence of the role of this efflux transporter in effectively restricting the brain penetration of its substrates across the human blood–brain barrier (BBB). This may not reflect the situation for weak ABCB1 substrates including several antidepressants, antiepileptic drugs, and neuroleptics, which exert central nervous system effects despite being transported by ABCB1. We performed PET with the weak ABCB1 substrate ^{11}C-metoclopramide in humans to elucidate the impact of ABCB1 function on its brain kinetics. **Methods:** Ten healthy male subjects underwent 2 consecutive ^{11}C-metoclopramide PET scans without and with ABCB1 inhibition using cyclosporine A (CsA). Pharmacokinetic modeling was performed to estimate the total volume of distribution (V_T) and the influx (K_1) and efflux (k_2) rate constants between plasma and selected brain regions. Furthermore, ^{11}C-metoclopramide washout from the brain was estimated by determining the elimination slope ($k_{E,brain}$) of the brain time–activity curves. **Results:** In baseline scans, ^{11}C-metoclopramide showed appreciable brain distribution (V_T = 2.11 ± 0.33 mL/cm^3). During CsA infusion, whole-brain gray matter V_T and K_1 were increased by 29% ± 17% and 9% ± 12%, respectively. K_2 was decreased by 15% ± 5%, consistent with a decrease in $k_{E,brain}$ (−32% ± 18%). The impact of CsA on outcome parameters was significant and similar across brain regions except for the pituitary gland, which is not protected by the BBB. **Conclusion:** Our results show for the first time that ABCB1 does not solely account for the "barrier" property of the BBB but also acts as a detoxifying system to limit the overall brain exposure to its substrates at the human blood–brain interface.

Key Words: blood-brain barrier; P-glycoprotein; ^{11}C-metoclopramide; PET

J Nucl Med 2019; 60:985–991
DOI: 10.2967/jnumed.118.219972

Central nervous system (CNS)–acting drugs are characterized by a large variability in pharmacologic response and tolerance between patients (*1–3*). Mechanisms for such variability remain incompletely understood and may imply differences in brain exposure (*4*). Before reaching the brain, drugs have to cross the blood–brain barrier (BBB) and variability in brain exposure may be related to variability in the extent by which drugs cross the BBB. The ATP-binding cassette (ABC) transporter P-glycoprotein (ABCB1) is an efflux transporter localized in the luminal membrane of brain capillary endothelial cells forming the BBB, which effectively restricts the blood-to-brain transfer of many drugs (*4*).

A large body of research has revealed that the BBB is a complex, dynamic interface, which may respond to pathophysiologic changes and play a role in disease progression (*5*). Disease-induced changes in ABCB1 function at the BBB may influence the neuropharmacokinetics and pharmacodynamics of CNS-acting ABCB1 substrates in humans. Global or localized induction of ABCB1 function at the BBB has been proposed as a mechanism contributing to pharmacoresistance whereas a decrease in ABCB1 function might be associated with a higher susceptibility to CNS adverse effects (*4*). Quantitative mapping of ABCB1 function at the human BBB is necessary to investigate ABCB1 function as a molecular determinant for inadequate therapeutic response to CNS-acting ABCB1 substrates in patients.

Systematic screening of current drugs and new chemical entities showed that many CNS-acting drugs are ABCB1 substrates (*6*). This includes some antidepressants (*7,8*), antipsychotics (*9,10*), antiepileptic drugs (*11*), opioids (*12*), as well as the antiemetic drug metoclopramide (*13*). Rodent experiments have shown that ABCB1 inhibition or genetic ABCB1 depletion increased their brain exposure and CNS effects (*6,8,10,12,14*). These compounds are classified as "weak" ABCB1 substrates based on their efflux ratios, assessed in vitro using standardized bidirectional transport assays (*13*). Compared with "avid" ABCB1 substrates, for which efflux ratios are higher, ABCB1 function seems to minimally restrict the brain penetration of weak substrates but may nonetheless play a role in controlling their brain kinetics.

PET imaging using radiolabeled analogs of drugs is a powerful method to study their brain kinetics and their transfer across the

Received Nov. 6, 2018; revision accepted Nov. 28, 2018.
For correspondence or reprints contact: Martin Bauer, Department of Clinical Pharmacology, Medical University of Vienna, A-1090 Vienna, Austria.
E-mail: martin.m.bauer@meduniwien.ac.at
*Contributed equally to this work.
Published online Jan. 10, 2019.

human BBB. In humans, pharmacologic ABCB1 inhibition using cyclosporine A (CsA) or tariquidar resulted in pronounced increases in the plasma-to-brain permeation of the avid ABCB1 substrates ^{11}C-verapamil, (*R*)-^{11}C-verapamil (*15,16*), and ^{11}C-*N*-desmethyl-loperamide (*17*). ^{11}C-metoclopramide is a recently developed weak ABCB1 substrate PET tracer (*18,19*). PET data obtained with ^{11}C-metoclopramide in nonhuman primates suggested a dual role of ABCB1 in limiting the brain entry (influx hindrance) and controlling the clearance of ^{11}C-metoclopramide from the brain into the blood (efflux enhancement) (*18,19*). An efflux enhancement role of ABCB1 has not been observed for avid ABCB1 substrate PET tracers (*15–17*), and it remains to be demonstrated whether this mechanism also exists at the human BBB.

In the present study, we assessed for the first time, to our knowledge, the impact of ABCB1 function on the brain kinetics of ^{11}C-metoclopramide in humans by performing PET scans without and with ABCB1 inhibition using a clinically validated infusion protocol of the ABCB1 inhibitor CsA (*15*).

MATERIALS AND METHODS

Ethics

The study was registered under European Union Drug Regulating Authorities Clinical Trials number 2017-000989-30 and was conducted according to good clinical practice standards. The study was approved by the local ethics committee and regulatory authority, and written informed consent was obtained from all subjects. Ten male subjects (mean age, 26 ± 4 y; mean weight, 73 ± 11 kg) were included in the study. Subjects were free of any medication for at least 14 d and judged as healthy based on clinical examination, routine blood and urine laboratory assessments, and urine drug screening.

Radiochemistry

^{11}C-metoclopramide was prepared from ^{11}C-carbon dioxide and *O*-desmethyl metoclopramide (good manufacturing practice quality; ABX) following a previously published procedure (*20*). For intravenous injection, ^{11}C-metoclopramide was formulated in phosphate-buffered saline solution containing 8.6% (v/v) ethanol. Molar activity at the time of radiotracer injection was 56 ± 30 GBq/μmol, and radiochemical purity was greater than 98%.

PET Experiments

PET scans were obtained on an Advance (GE Healthcare) standalone PET scanner. Each subject underwent 2 consecutive, dynamic 60-min PET scans on 1 study day. During each of the 2 scans, starting with ^{11}C-metoclopramide bolus injection (scan 1, 379 ± 45 MBq; scan 2, 393 ± 13 MBq, $P = 0.385$, corresponding to 14 ± 9 and 13 ± 7 nmol of unlabeled metoclopramide, respectively, $P = 0.698$) over approximately 20 s, arterial blood samples (2 mL) were collected approximately every 7 s for the first 2.5 min followed by 9-mL samples at 3.5, 5, 10, 20, 30, 40, and 60 min after radiotracer injection. For ABCB1 inhibition during the second PET scan, a previously described CsA infusion protocol was used (*15*). CsA (Sandimmun, 50-mg concentrate for infusion; Novartis Pharma GmbH) was administered as an intravenous infusion over 2 h at a rate of 2.5 mg/kg of body weight/h. The infusion was started at 1 h before start of the second PET scan and was maintained for the duration of the second PET scan. One blood sample (4.5 mL) was collected at the end of the second PET scan, concurrent with the end of the CsA infusion, and stored at −80°C until analysis of CsA concentrations. The plasma samples collected at 5, 10, 20, 30, and 40 min after radiotracer injection were analyzed for radiolabeled metabolites of ^{11}C-metoclopramide.

Determination of Parent ^{11}C-Metoclopramide in Plasma

Plasma samples (830 μL) collected at 5, 10, 20, 30 and 40 min after ^{11}C-metoclopramide injection were mixed with acetonitrile (600 μL) and vortexed to precipitate plasma proteins. After addition of water (600 μL) and phosphate-buffered saline (10-fold concentrate, pH 7.4, 100 μL), samples were centrifuged (4 min, 15,000*g*, 4°C) and the protein pellet and supernatant were separately counted in a gamma counter to determine the recovery of radioactivity, which was for the 10 min time point 87% ± 2% for the baseline scan and 88% ± 2% for the CsA scan ($n = 9$). The supernatant (1.5 mL) was then injected into the high-performance liquid chromatography (HPLC) system. An Atlantis T3 OBD HPLC column (250 × 10 mm, 10 μm, Waters, Austria) equipped with a precolumn (Atlantis T3 Prep Guard Cartridge, 10 × 10 mm, 10 μm) was eluted with a mixture of 25 mM aqueous ammonium acetate (solvent A) and acetonitrile (solvent B). A linear gradient from 20% to 30% of solvent B over 5.5 min (total run length, 10 min) was applied to the column at a flow rate of 5 mL/min. On this HPLC system ^{11}C-metoclopramide and its radiolabeled metabolites eluted with retention times of approximately 8.5 and 4 min, respectively. HPLC eluates were collected in 1-min fractions, which were counted for radioactivity in a gamma counter. The measured fractions were corrected for radioactive decay to determine the percentage of unmetabolized ^{11}C-metoclopramide in plasma at different time points.

A monoexponential decay function was fitted to the percentage of unmetabolized ^{11}C-metoclopramide versus time and then applied to the corresponding decay-corrected total radioactivity counts in plasma to derive a metabolite-corrected arterial input function (*19*). An arterial plasma sample was obtained immediately before each ^{11}C-metoclopramide injection to assess the fraction of free (i.e., non–protein bound) ^{11}C-metoclopramide in plasma (f_P) using ultrafiltration as previously described (*19*).

Determination of CsA Concentrations in Blood

The concentration of CsA in whole blood was determined by HPLC with minor modifications as described previously (*21*). Briefly, after hemolysis of 1-mL whole blood by the addition of a mixture of zinc sulfate/methanol (65:35, w/v; 2 mL), 50 μL (1.0 μg) of cyclosporine D (Cayman Chemical) were added as the internal standard. After centrifugation (5 min, 3,000*g*), the supernatant was passed through an Oasis HLB 1 cc SPE cartridge (30 mg; Waters Corporation), which had been equilibrated with 2 mL of methanol and water (pH 3.0), respectively. The column was washed with methanol in water (50%, v/v; 2.3 mL) and heptane (0.5 mL), and CsA was eluted with ethanol (100%, 300 μL). The eluate was mixed with 100 μL of water (pH 3.0) and 1 mL of heptane and centrifuged for 5 min at 3,000*g*. An aliquot (80 μL) of the aqueous phase was injected onto the HPLC column. HPLC was performed using a Dionex "UltiMate 3000" system (Dionex Corp.) with ultraviolet detection at 205 nm. Chromatographic separation was carried out at 75°C on a Hypersil BDS-C18 column (5 μm, 250 × 4.6 mm, Thermo Fisher Scientific, Inc.), preceded by a Hypersil BDS-C18 precolumn (5 μm, 10 × 4.6 mm). The mobile phase consisted of a continuous gradient, mixed from solvent A (acetonitrile in water [35:75, v/v]) and solvent B (acetonitrile in water [85:15, v/v]). The column was equilibrated with 45% solvent B at time 0; after injection of the sample (80 μL), the content of solvent B was linearly increased to 93% at 19 min. Subsequently, the percentage of solvent B was decreased to 45% within 2 min, to equilibrate the column for 8 min before application of the next sample. Linearity was tested by assaying drug-free whole blood spiked with 0.1, 0.5, 2.5, and 10 μg of CsA. The calibration curve for CsA in blood was linear over the tested concentration range (correlation coefficient, 0.985). Quantification of CsA was based on the comparison of CsA/cyclosporine D ratios.

Data Analysis

Individual T1-weighted MR images acquired on a MAGNETOM Skyra 3.0 T scanner (Siemens Medical Solutions) were segmented with SPM12 (Statistical Parametric Mapping, Wellcome Trust Centre for Neuroimaging) to define gray and white matter. As previously described, the adult brain maximum probability map ("Hammersmith atlas"; n30r83) was used to define whole-brain gray matter, white matter, middle frontal gyrus, putamen, caudate nucleus, medial occipital lobe, and cerebellum as regions of interest (ROIs) (*22,23*). In addition, the pituitary gland (ROI volume, 0.22 ± 0.15 cm^3), which is not protected by a functional BBB, was manually outlined on individual MR images, which were coregistered to the PET summation images using PMOD software (version 3.6; PMOD Technologies Ltd.). ROIs were transferred to the respective dynamic PET datasets to extract time–activity curves. The time–activity curves were normalized to the injected radioactivity amount per body weight and expressed in units of SUV (SUV = [radioactivity per g of tissue/injected radioactivity] × body weight), and the following descriptive pharmacokinetic parameters were determined: maximum concentration (C_{max}, SUV, calculated from time points > 1.25 min to exclude the arterial blood peak in the brain), the time of C_{max} (T_{max}, min), the concentration at 55 min after radiotracer injection ($C_{55\ min}$, SUV), and the area under the curve from 0 to 60 min after radiotracer injection (AUC_{brain}, SUV × min). In addition, the elimination slope for radioactivity washout from the brain ($k_{E,brain}$, 1/min) was estimated by linear regression analysis of the log-transformed brain time–activity curves from 35 to 60 min after radiotracer injection.

The PMOD Kinetic Modeling tool was used to analyze the PET and metabolite-corrected plasma data using a reversible 1-tissue-2-rate constant (1T2K) compartmental model to estimate the rate constants for radioactivity transfer from plasma into brain (K_1, mL/(cm^3 × min)) and from brain into plasma (k_2, 1/min) and the total volume of distribution ($V_T = K_1/k_2$, mL/cm^3). The fractional arterial blood volume in the brain (V_b) was included as a fitting parameter. In addition, parametric images for K_1, k_2, and V_T were calculated for both conditions with the PMOD Pixelwise Modeling tool.

From the metabolite-corrected plasma time–activity curves expressed in SUV units, C_{max} (SUV), T_{max} (min), AUC_{plasma} from 0 to 60 min after radiotracer injection (SUV × min), and the elimination slope from 30 to 60 min after injection ($k_{E,plasma}$, 1/min) were calculated.

Statistical Analysis

Statistical analysis was performed using Prism Software (version 7.04; GraphPad Software). Outcome parameters were tested for normal distribution and compared between scans using a 2-sided, paired *t* test. Regional differences were determined for each outcome parameter with 1-way ANOVA followed by a Tukey's multiple comparison test. To assess correlations, the Pearson correlation coefficient *r* was determined. The level of statistical significance was set to a *P* value of less than 0.05. All values are expressed as mean ± SD.

RESULTS

Tolerance of Procedure

There were no adverse or clinically detectable pharmacologic effects related to the radiotracer administered in any of the 10 subjects. All subjects experienced mild, reversible hot flashes within minutes after start of CsA infusion. Further mild and reversible adverse events recorded were headache (n = 3), nausea (n = 1), and local exanthema (n = 1).

Brain Kinetics

In baseline scans, there was substantial brain uptake of radioactivity, which was rather homogeneously distributed throughout the brain (Fig. 1A). During CsA infusion a slight increase in brain radioactivity was observed in some subjects (Fig. 1A). In Supplemental Table 1 (supplemental materials are available at http://jnm.snmjournals.org), descriptive pharmacokinetic parameters are summarized for all tested brain regions. The maximum radioactivity concentration (C_{max}) in the brain was similar under both conditions, but the time of C_{max} (T_{max}) was in all brain regions later during ABCB1 inhibition than in baseline scans. Conversely, brain concentrations measured at the end of the PET acquisition ($C_{55\ min}$) were significantly higher during ABCB1 inhibition in several of the tested brain regions (Supplemental Table 1; Fig. 1B). Brain exposure to radioactivity (AUC_{brain}) was not significantly different between the 2 scans in any of the investigated brain regions. With the exception of the pituitary gland, the elimination slope of radioactivity washout from the brain ($k_{E,brain}$) was significantly reduced during CsA infusion ($P < 0.01$; range, −26% for cerebellum to −90% for white matter) (Supplemental Table 1, Supplemental Fig. 1A). We also determined $k_{E,brain}$ from 12.5 to 60 min after radiotracer injection, and these values showed across all gray matter ROIs an excellent correlation with $k_{E,brain}$ values

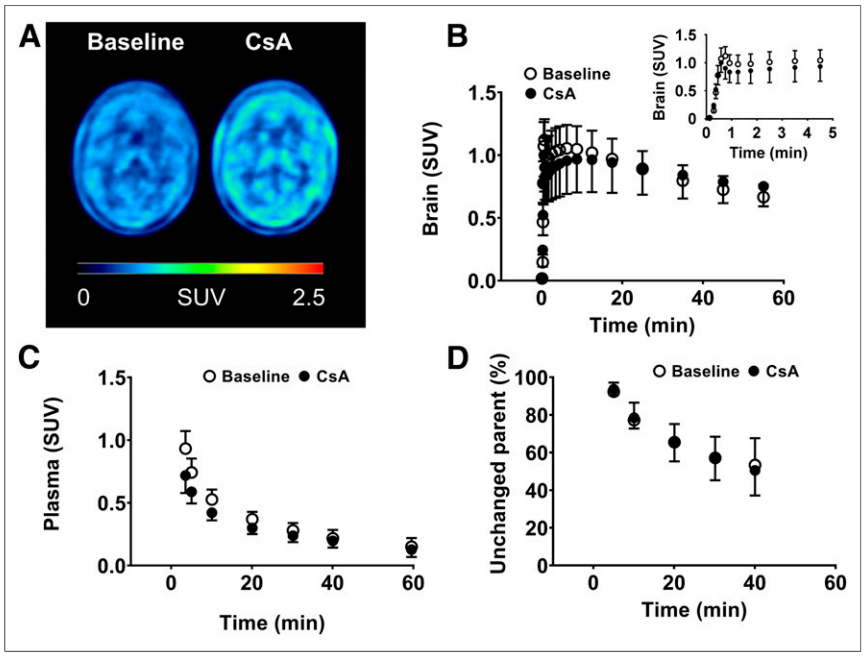

FIGURE 1. (A) Representative PET average images of brain (0–60 min) for scans without (baseline) and with CsA infusion. (B) Mean (±SD, n = 10) time–activity curves in whole-brain gray matter for both conditions, with insert showing early data after radiotracer injection. (C) Mean (±SD, n = 10) time–activity curves of unmetabolized ^{11}C-metoclopramide in arterial plasma for both conditions. (D) Percentage of unchanged ^{11}C-metoclopramide in arterial plasma over time.

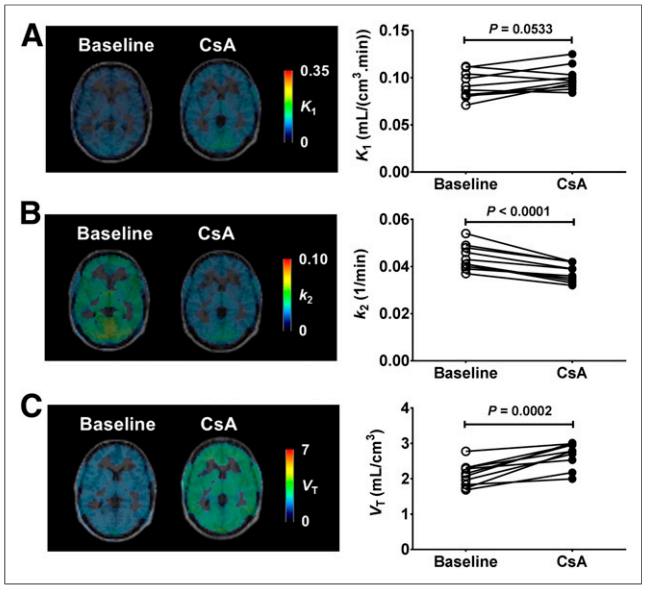

FIGURE 2. Representative MR image–coregistered parametric images from 1 subject and individual parameter values in whole-brain gray matter for scans without (baseline) and with CsA infusion for K_1 (A), k_2 (B), and V_T (C). Shown *P* values are from 2-sided, paired *t* test.

calculated from 35 to 60 min after radiotracer injection (r = 0.9018, $P < 0.0001$).

Plasma Kinetics

Plasma concentrations of ^{11}C-metoclopramide peaked rapidly, followed by a washout with a mean half-life of 38 ± 21 min (Fig. 1C). At 40 min after radiotracer injection, the percentage of unmetabolized ^{11}C-metoclopramide in plasma was 53% ± 14% for scan 1 and 51% ± 13% for scan 2 (P = 0.102) (Fig. 1D). These values were 92% ± 5% and 94% ± 3% at 5 min (P = 0.455), 77% ± 9% and 78% ± 6% at 10 min (P = 0.629), 65% ± 10% and 65% ± 10% at 20 min (P = 0.968), and 57% ± 11% and 57% ± 12% at 30 min (P = 0.845) for scan 1 and scan 2, respectively. Both plasma C_{max} and T_{max} values were significantly different between the 2 scans (C_{max} [SUV], scan 1: 18.5 ± 3.4, scan 2: 15.2 ± 2.6, P = 0.0001; T_{max} [min], scan 1: 0.63 ± 0.07, scan 2: 0.54 ± 0.04, P = 0.0049). AUC_{plasma} was significantly lower in scan 2 (AUC_{plasma} [SUV × min], scan 1: 31 ± 5, scan 2: 25 ± 4, P = 0.0002). $K_{E,plasma}$ was not significantly different between the 2 scans (P = 0.3163) (Supplemental Fig. 1B). No correlation was found between the percentage change in $k_{E,brain}$ and $k_{E,plasma}$ in scan 2 (Supplemental Fig. 1C). The free fraction (f_p) of ^{11}C-metoclopramide in plasma was 0.22 ± 0.6 in the first scan and 0.26 ± 0.6 in the second scan ($P < 0.0001$). CsA concentration in blood could be determined in 9 subjects. Mean CsA concentration in blood at the end of the PET scan was 3.4 ± 0.4 μmol/L (range, 2.5–3.9 μmol/L).

Kinetic Modeling

A 1T2K model was applied to estimate the distribution of radioactivity from plasma into the brain under the 2 tested conditions. Exemplary fits for each condition are shown in Supplemental Figure 2. A 2-tissue-4-rate constant compartmental model was also tried to model the data but failed to provide estimates for all 4 rate constants in 6 of the 20 datasets (data not shown). Outcome parameters from kinetic modeling are summarized in Supplemental Table 2. Across all gray matter ROIs, V_T was negatively correlated (r = −0.3048, P = 0.0013) and k_2 was positively correlated (r = 0.4034, $P < 0.0001$) with the respective $k_{E,brain}$ values, whereas K_1 showed no correlation with $k_{E,brain}$ (r = 0.1089, P = 0.2620). In all studied brain regions except white matter, there was appreciable brain uptake of radioactivity in baseline scans ($V_T \geq 2$ mL/cm^3). The highest radioactivity uptake was observed in the pituitary gland, a region located outside the functional BBB. In the putamen, a brain region that is rich in dopamine D_2 receptors (D_2R), mean V_T was 24% higher as compared with whole-brain gray matter, but this difference was not statistically significant (P = 0.789, Supplemental Table 2, Supplemental Fig. 3).

In all studied brain regions except the pituitary gland, V_T was significantly increased during ABCB1 inhibition. Increases in V_T ($= K_1/k_2$) were caused by decreases in k_2, which was significantly reduced in scan 2 in all tested brain regions, and less pronounced increases in K_1, which were only in some of the investigated brain regions statistically significant (Supplemental Table 2). In the pituitary gland, there were no significant changes in K_1 and k_2 values between the 2 conditions. In Figure 2, parametric PET images and modeling outcome parameters are shown for both scans for the whole-brain gray matter region. In this region, V_T was increased by 29% ± 17% (P = 0.0002), K_1 was increased by 9% ± 12% (P = 0.0533), and k_2 was decreased by 15% ± 5% ($P < 0.0001$) during ABCB1 inhibition (Fig. 2). The reduction in k_2 was consistent with a 32% ± 18% decrease in $k_{E,brain}$. In Figure 3, the percentage changes in modeling outcome parameters in scan 2 are compared for all tested gray matter ROIs. No statistically significant differences in the response to CsA were found between the different brain regions.

DISCUSSION

The present study reports the first assessment of ^{11}C-metoclopramide in humans. In vitro studies have shown that metoclopramide is a

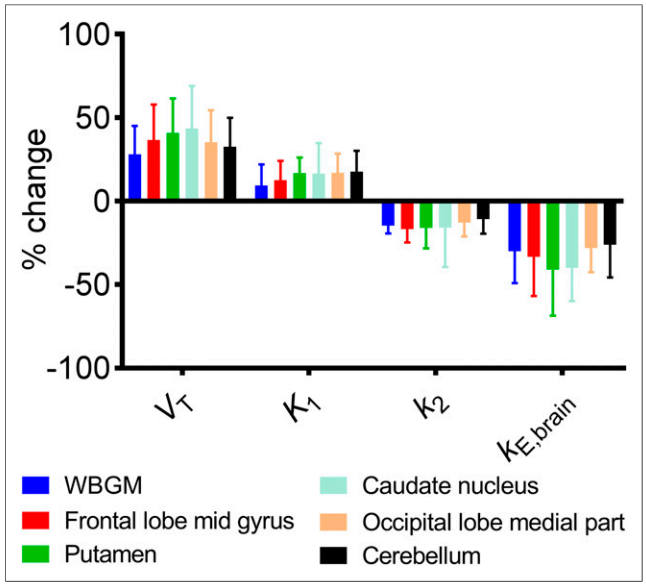

FIGURE 3. Mean (+SD, n = 10) percentage change of model outcome parameters K_1, k_2, V_T, and $k_{E,brain}$ in response to CsA infusion in different brain regions. WBGM = whole-brain gray matter. One-way ANOVA with Tukey's multiple comparison test revealed no significant differences for within-group comparisons.

weak substrate of human ABCB1 (*13*), but not of breast cancer resistance protein (ABCG2), the other major ABC transporter expressed at the human BBB (*18*). Moreover, previous preclinical experiments suggested that ^{11}C-metoclopramide is a suitable ABCB1 PET tracer without brain penetration of radiolabeled metabolites and with negligible interaction with CNS targets other than ABCB1 (*18,19*). In humans, one major unidentified polar radiolabeled metabolite of ^{11}C-metoclopramide was observed in plasma, which eluted with a comparable high-performance liquid chromatography retention time as in rats and in nonhuman primates (*18,19*). Metabolism of ^{11}C-metoclopramide appeared to be considerably slower in humans than previously reported in rats and nonhuman primates (*18,19*).

CNS effects of metoclopramide reported in patients suggest a substantial brain distribution (*24*), which is in accordance with the appreciable brain uptake of radioactivity observed in PET scans without ABCB1 inhibition (Fig. 1A). Functional MRI studies have shown that the CNS effects of metoclopramide are localized in the putamen, consistent with D_2R antagonism, and in the insular cortices and anterior temporal lobes (*25*). In agreement with this, we found moderately higher V_T values in the putamen than in the whole-brain gray matter, suggesting some degree of binding of ^{11}C-metoclopramide to D_2R. Apart from a weak accumulation in the basal ganglia, we observed a rather homogeneous distribution across different brain regions, which suggests a negligible contribution of specific binding of ^{11}C-metoclopramide to the overall PET signal and a predominantly nonspecific retention mechanism in brain parenchyma. This is in accordance with previously performed preclinical experiments, in which coinjection of unlabeled metoclopramide failed to reveal specific binding of ^{11}C-metoclopramide in the brain (*18,19*).

In previous preclinical studies, tariquidar has been used as a potent and well-tolerated ABCB1 inhibitor (*18,19*). As tariquidar is no longer available for clinical use, we used in this study CsA as an ABCB1 inhibitor. We used the same CsA administration protocol as has been used before to enhance brain uptake of the avid ABCB1 substrate ^{11}C-verapamil in humans (*15*). CsA infusion resulted in a significant increase in the brain distribution (V_T) of ^{11}C-metoclopramide, which confirmed transport by ABCB1 at the human BBB. V_T/f_P, which takes the impact of CsA on plasma protein binding of ^{11}C-metoclopramide into account, was also significantly increased in most brain regions after ABCB1 inhibition (Supplemental Table 2). ABCB1 function can therefore be considered as a determinant of the brain exposure to metoclopramide. An increase in V_T after ABCB1 inhibition was not observed in the pituitary gland, consistent with a lack of ABCB1-mediated efflux in this brain region (*16,17*). The small chemoreceptor trigger zone of the area postrema, which is the known pharmacologic target tissue of metoclopramide in the brain, is also not protected by the BBB (*26*). ABCB1 function may thus preferentially control the CNS side effects of metoclopramide (akathisia and dystonia), which are associated with the blockage of D_2R in the striatum (*24*), rather than its therapeutic (antiemetic) effect.

The selected dose of CsA induced an approximately 30% increase in the whole-brain gray matter V_T of ^{11}C-metoclopramide. After ABCB1 inhibition, ^{11}C-metoclopramide V_T remained approximately 3-fold lower than in the pituitary gland, suggesting that only partial ABCB1 inhibition could be achieved using the selected dose of CsA. This assumption is also supported by the observation that ^{11}C-metoclopramide brain V_T increase was higher (2-fold increase) in a previously published nonhuman primate study, in which tariquidar was used as a more potent ABCB1 inhibitor than CsA (*19*). Kinetic modeling using a 1T2K model revealed that the increase in V_T was due to a 9% increase in K_1 and a 15% decrease in k_2 (Fig. 2). Muzi et al. reported an approximately 70% increase in ^{11}C-verapamil brain V_T using the same ABCB1 inhibition protocol in healthy volunteers (*15*). This increase in V_T was consistent with an approximately 70% increase in K_1, with a limited impact of CsA infusion on cerebral blood flow (13% increase) (*15*). The authors could not find any impact of CsA on ^{11}C-verapamil k_2 in the 1T2K model. Compared with verapamil (in vitro efflux ratio = 2.1), metoclopramide is a weaker ABCB1 substrate (efflux ratio = 1.4, measured under the same conditions) (*13*). The low baseline brain distribution of ^{11}C-verapamil (V_T = 0.59 vs. 2.1 ± 0.3 mL/cm^3 for ^{11}C-metoclopramide), in combination with a possible brain uptake of radiolabeled metabolites (*27*), made it difficult to estimate the impact of ABCB1 on the efflux transport of ^{11}C-verapamil from the brain. In contrast, for ^{11}C-metoclopramide the impact of ABCB1 function predominated on k_2 rather than on K_1. This may be due to the better ability of ^{11}C-metoclopramide to cross the BBB as compared with ^{11}C-verapamil and a putative lack of brain-penetrant radiolabeled metabolites, resulting in an effect of ABCB1 on the efflux clearance of ^{11}C-metoclopramide across the BBB. Focusing on the influx hindrance role of ABCB1 at the BBB may thus underestimate the overall impact of ABCB1 on the brain distribution and exposure to its substrates.

We found no regional differences in changes in ^{11}C-metoclopramide modeling outcome parameters in response to ABCB1 inhibition in different gray matter ROIs (Fig. 3), which was consistent with earlier reports of negligible regional differences in ABCB1 function in the healthy human brain (*28,29*). In white matter, there were greater changes in modeling outcome parameters in response to CsA administration as compared with the gray matter ROIs (Supplemental Table 2), which may, however, be related to partial-volume effects.

Infusion of CsA significantly reduced the ^{11}C-metoclopramide plasma exposure (AUC_{plasma}) but did not change the elimination slope of parent ^{11}C-metoclopramide from plasma ($k_{E,plasma}$) (Supplemental Fig. 1B). As a change in the arterial input function will have an impact on the brain PET signal, the brain exposure to radioactivity (AUC_{brain}) could not be used in our study as a surrogate parameter to measure ABCB1 function at the BBB. Therefore the arterial input function needed to be considered to estimate the distribution of ^{11}C-metoclopramide from the plasma into the brain using full kinetic modeling. Arterial blood sampling is sometimes difficult to perform in patients. $K_{E,brain}$, which can be directly determined from the brain time–activity curves without the need to consider the arterial input function, was significantly reduced by 32% after ABCB1 inhibition. This change in $k_{E,brain}$ was independent of the corresponding plasma kinetics (Supplemental Fig. 1C). Moreover, the magnitude of the change in $k_{E,brain}$ after ABCB1 inhibition was comparable to that of V_T, obtained with full kinetic modeling. Consequently, $k_{E,brain}$ appears as a suitable parameter to noninvasively estimate ABCB1 function at the BBB in humans without the need for arterial blood sampling, similar to our previous findings in nonhuman primates (*19*).

Of particular interest in neuropharmacology is the role of ABCB1 in insufficient response to CNS-acting drugs and in pharmacoresistance. This may be particularly relevant in epilepsy and major depression as many antiepileptic drugs and antidepressants are weak ABCB1 substrates (*4*). Currently available avid ABCB1 substrates for PET (^{11}C-verapamil, (*R*)-^{11}C-verapamil, and ^{11}C-*N*-desmethyl-loperamide) lack the sensitivity to detect moderate changes in ABCB1 function at the BBB, due to the ability of ABCB1 to functionally compensate

moderate changes in its expression (*30*). Therefore, a 2-scan PET protocol involving a baseline scan and a second scan after intravenous administration of tariquidar at a dose that partially inhibits ABCB1 at the BBB was used to reveal a localized ABCB1 induction in the brains of patients with therapy-refractory epilepsy (*31*). This PET protocol is complex and limited by the lack of availability of tariquidar for clinical use. It can be hypothesized that weak ABCB1 substrates may be better suited to detect moderate changes in ABCB1 function at the BBB than avid substrates using a single scan, without the need to administer an ABCB1 inhibitor. Prior efforts have been made to identify weak ABCB1 substrate radiotracers for PET imaging of ABCB1 function at the BBB (e.g., ^{18}F-MC225, ^{18}F-MPPF, ^{18}F-FCWAY, and ^{11}C-phenytoin) (*32–35*). However, none of these compounds has so far been applied to study ABCB1 function in patients to confirm the hypothesis that they possess a higher sensitivity to assess cerebral ABCB1 function than avid ABCB1 substrates. In addition, further factors, such as species differences in substrate recognition (^{18}F-MPPF) or specific binding in the brain (i.e., to 5-HT$_{1A}$ receptors: ^{18}F-MPPF and ^{18}F-FCWAY), may restrict their applicability as ABCB1 PET probes (*32–35*). For ^{11}C-metoclopramide, there was probably some binding to D_2R in the putamen, which is the region with the highest D_2R density in the brain (*36*). However, V_T in the putamen was only 37% higher as compared with the cerebellum, which lacks D_2R. This suggests that the D_2R affinity of metoclopramide, which explains the CNS effects at pharmacologic doses, is not sufficiently high to clearly distinguish the specific binding of ^{11}C-metoclopramide from its predominantly nonspecific binding to brain parenchyma. On the basis of this, it seems unlikely that D_2R binding will exert an appreciable impact on the kinetics of ^{11}C-metoclopramide in brain regions other than the basal ganglia. Coinjection of ^{11}C-metoclopramide with a pharmacologic dose of unlabeled metoclopramide, as previously reported in rodents and nonhuman primates (*18,19*), will be helpful to address a possible confounding effect of specific binding on the quantification of ABCB1 function in D_2R-rich brain regions.

CONCLUSION

We performed for the first time, to our knowledge, ^{11}C-metoclopramide PET imaging in humans to reveal the impact of ABCB1 function on the brain kinetics of this representative weak ABCB1 substrate. We showed that ABCB1 function both hindered the influx and enhanced the efflux of ^{11}C-metoclopramide across the BBB. Our results show for the first time that ABCB1 does not solely account for the "barrier" property of the BBB but also acts as a detoxifying system to limit the overall brain exposure to its substrates at the human blood-brain interface. Efflux enhancement by ABCB1 may play a critical role in controlling both therapeutic effects and side effects of CNS-acting drugs in patients. In comparison to previously described radiotracers, ^{11}C-metoclopramide benefits from a substantial baseline brain uptake. Moreover, the suitable pharmacokinetic properties of ^{11}C-metoclopramide allow for a minimally invasive estimation of ABCB1 function at the human BBB. ^{11}C-metoclopramide PET may offer the opportunity to comprehensively assess the contribution of ABCB1 to pharmacoresistance in patients with brain diseases.

DISCLOSURE

This work was supported by the Austrian Science Fund (FWF) (grants KLI 694-B30, KLI 480-B30). No other potential conflict of interest relevant to this article was reported.

ACKNOWLEDGMENTS

We thank Harald Ibeschitz, Ingrid Leitinger, and the other staff members of the PET center at the Division of Nuclear Medicine for their smooth cooperation in this study, and Johann Stanek for technical support. Ulrich Sauerzopf (Department of Psychiatry and Psychotherapy) is acknowledged for help with the parametric analysis of the PET data.

REFERENCES

1. Zhang JP, Malhotra AK. Pharmacogenetics and antipsychotics: therapeutic efficacy and side effects prediction. *Expert Opin Drug Metab Toxicol.* 2011;7:9–37.
2. Kwan P, Schachter SC, Brodie MJ. Drug-resistant epilepsy. *N Engl J Med.* 2011;365:919–926.
3. Kato M, Serretti A. Review and meta-analysis of antidepressant pharmacogenetic findings in major depressive disorder. *Mol Psychiatry.* 2010;15:473–500.
4. Löscher W, Potschka H. Drug resistance in brain diseases and the role of drug efflux transporters. *Nat Rev Neurosci.* 2005;6:591–602.
5. Obermeier B, Daneman R, Ransohoff RM. Development, maintenance and disruption of the blood-brain barrier. *Nat Med.* 2013;19:1584–1596.
6. Doran A, Obach RS, Smith BJ, et al. The impact of P-glycoprotein on the disposition of drugs targeted for indications of the central nervous system: evaluation using the MDR1A/1B knockout mouse model. *Drug Metab Dispos.* 2005;33:165–174.
7. Uhr M, Steckler T, Yassouridis A, Holsboer F. Penetration of amitriptyline, but not of fluoxetine, into brain is enhanced in mice with blood-brain barrier deficiency due to mdr1a P-glycoprotein gene disruption. *Neuropsychopharmacology.* 2000;22:380–387.
8. O'Brien FE, O'Connor RM, Clarke G, Dinan TG, Griffin BT, Cryan JF. P-glycoprotein inhibition increases the brain distribution and antidepressant-like activity of escitalopram in rodents. *Neuropsychopharmacology.* 2013;38:2209–2219.
9. Schmitt U, Kirschbaum KM, Poller B, et al. In vitro P-glycoprotein efflux inhibition by atypical antipsychotics is in vivo nicely reflected by pharmacodynamic but less by pharmacokinetic changes. *Pharmacol Biochem Behav.* 2012;102:312–320.
10. Kirschbaum KM, Henken S, Hiemke C, Schmitt U. Pharmacodynamic consequences of P-glycoprotein-dependent pharmacokinetics of risperidone and haloperidol in mice. *Behav Brain Res.* 2008;188:298–303.
11. Luna-Tortós C, Fedrowitz M, Löscher W. Several major antiepileptic drugs are substrates for human P-glycoprotein. *Neuropharmacology.* 2008;55:1364–1375.
12. Hassan HE, Myers AL, Coop A, Eddington ND. Differential involvement of P-glycoprotein (ABCB1) in permeability, tissue distribution, and antinociceptive activity of methadone, buprenorphine, and diprenorphine: in vitro and in vivo evaluation. *J Pharm Sci.* 2009;98:4928–4940.
13. Feng B, Mills JB, Davidson RE, et al. In vitro P-glycoprotein assays to predict the in vivo interactions of P-glycoprotein with drugs in the central nervous system. *Drug Metab Dispos.* 2008;36:268–275.
14. Nakanishi H, Yonezawa A, Matsubara K, Yano I. Impact of P-glycoprotein and breast cancer resistance protein on the brain distribution of antiepileptic drugs in knockout mouse models. *Eur J Pharmacol.* 2013;710:20–28.
15. Muzi M, Mankoff DA, Link JM, et al. Imaging of cyclosporine inhibition of P-glycoprotein activity using ^{11}C-verapamil in the brain: studies of healthy humans. *J Nucl Med.* 2009;50:1267–1275.
16. Bauer M, Karch R, Zeitlinger M, et al. Approaching complete inhibition of P-glycoprotein at the human blood-brain barrier: an (*R*)-[^{11}C]verapamil PET study. *J Cereb Blood Flow Metab.* 2015;35:743–746.
17. Kreisl WC, Bhatia R, Morse CL, et al. Increased permeability-glycoprotein inhibition at the human blood-brain barrier can be safely achieved by performing PET during peak plasma concentrations of tariquidar. *J Nucl Med.* 2015;56:82–87.
18. Pottier G, Marie S, Goutal S, et al. Imaging the impact of the P-glycoprotein (ABCB1) function on the brain kinetics of metoclopramide. *J Nucl Med.* 2016;57:309–314.
19. Auvity S, Caillé F, Marie S, et al. P-glycoprotein (ABCB1) inhibits the influx and increases the efflux of ^{11}C-metoclopramide across the blood-brain barrier: a PET study on non-human primates. *J Nucl Med.* 2018;59:1609–1615.
20. Caillé F, Goutal S, Marie S, et al. Positron emission tomography imaging reveals an importance of saturable liver uptake transport for the pharmacokinetics of metoclopramide. *Contrast Media Mol Imaging.* 2018;2018:7310146.

21. Hamwi A, Salomon A, Steinbrugger R, Fritzer-Szekeres M, Jager W, Szekeres T. Cyclosporine metabolism in patients after kidney, bone marrow, heart-lung, and liver transplantation in the early and late posttransplant periods. *Am J Clin Pathol.* 2000;114:536–543.
22. Hammers A, Allom R, Koepp MJ, et al. Three-dimensional maximum probability atlas of the human brain, with particular reference to the temporal lobe. *Hum Brain Mapp.* 2003;19:224–247.
23. Bauer M, Karch R, Zeitlinger M, et al. Interaction of ^{11}C-tariquidar and ^{11}C-elacridar with P-glycoprotein and breast cancer resistance protein at the human blood-brain barrier. *J Nucl Med.* 2013;54:1181–1187.
24. Pasricha PJ, Pehlivanov N, Sugumar A, Jankovic J. Drug insight: from disturbed motility to disordered movement–a review of the clinical benefits and medicolegal risks of metoclopramide. *Nat Clin Pract Gastroenterol Hepatol.* 2006;3:138–148.
25. Fernández-Seara MA, Aznarez-Sanado M, Mengual E, Irigoyen J, Heukamp F, Pastor MA. Effects on resting cerebral blood flow and functional connectivity induced by metoclopramide: a perfusion MRI study in healthy volunteers. *Br J Pharmacol.* 2011;163:1639–1652.
26. Kiecker C. The origins of the circumventricular organs. *J Anat.* 2018;232:540–553.
27. Luurtsema G, Molthoff CF, Schuit RC, Windhorst AD, Lammertsma AA, Franssen EJ. Evaluation of (*R*)-[^{11}C]verapamil as PET tracer of P-glycoprotein function in the blood-brain barrier: kinetics and metabolism in the rat. *Nucl Med Biol.* 2005;32:87–93.
28. Eyal S, Ke B, Muzi M, et al. Regional P-glycoprotein activity and inhibition at the human blood-brain barrier as imaged by positron emission tomography. *Clin Pharmacol Ther.* 2010;87:579–585.
29. Bauer M, Karch R, Neumann F, et al. Assessment of regional differences in tariquidar-induced P-glycoprotein modulation at the human blood-brain barrier. *J Cereb Blood Flow Metab.* 2010;30:510–515.
30. Wanek T, Römermann K, Mairinger S, et al. Factors governing p-glycoprotein-mediated drug-drug interactions at the blood-brain barrier measured with positron emission tomography. *Mol Pharm.* 2015;12:3214–3225.
31. Feldmann M, Asselin M-C, Liu J, et al. P-glycoprotein expression and function in patients with temporal lobe epilepsy: a case-control study. *Lancet Neurol.* 2013;12:777–785.
32. Savolainen H, Windhorst AD, Elsinga PH, et al. Evaluation of [^{18}F]MC225 as a PET radiotracer for measuring P-glycoprotein function at the blood-brain barrier in rats: kinetics, metabolism, and selectivity. *J Cereb Blood Flow Metab.* 2017;37:1286–1298.
33. Mansor S, Boellaard R, Froklage FE, et al. Quantification of dynamic ^{11}C-phenytoin PET studies. *J Nucl Med.* 2015;56:1372–1377.
34. Liow JS, Zoghbi SS, Hu S, et al. ^{18}F-FCWAY, a serotonin 1A receptor radioligand, is a substrate for efflux transport at the human blood-brain barrier. *Neuroimage.* 2016;138:134–140.
35. Tournier N, Cisternino S, Peyronneau MA, et al. Discrepancies in the P-glycoprotein-mediated transport of ^{18}F-MPPF: a pharmacokinetic study in mice and non-human primates. *Pharm Res.* 2012;29:2468–2476.
36. Camps M, Cortes R, Gueye B, Probst A, Palacios JM. Dopamine receptors in human brain: autoradiographic distribution of D_2 sites. *Neuroscience.* 1989;28: 275–290.